The crystallographic phase transition for a ferric thiosemicarbazone spin crossover complex studied by X-ray powder diffraction†

Sébastien Floquet,*[ab] Nathalie Guillou,[b] Philippe Négrier,[c] Eric Rivière[a] and Marie-Laure Boillot*[a]

Received (in Montpellier, France) 13th April 2006, Accepted 9th August 2006
First published as an Advance Article on the web 24th August 2006
DOI: 10.1039/b605326b

The crystal structure of a spin-transition compound, namely the thiosemicarbazone ferric complex $Li[Fe(5BrThsa)_2]\cdot H_2O$, was solved from powder X-ray diffraction data at temperatures where the high-spin (373 K) and low-spin (150 K) phases prevail. The methodology is based on traditional approaches (direct methods) combined with direct space strategy. Both phases crystallise in the monoclinic system $P2_1/c$. At 373 K, the characteristics of the $[FeN_2O_2S_2]$ coordination core are consistent with those reported for high-spin iron(III) thiosemicarbazone complexes: a distorted coordination polyhedron and non-equivalent metal–ligand bond lengths. When the temperature is reduced to 150 K, a decrease of the β angle from *ca.* 101° (373 K) to *ca.* 90° (150 K) is the only major modification of the cell parameters. The low-spin molecular structure reveals significant differences in bond lengths and bond angles compared to the high-spin structure. Finally, an extended hydrogen-bond network is implicated in the cooperative phase transition, as supported by strong intermolecular contacts between the ferric complexes and the water molecules and the crystallographic phase transition is associated with pronounced lattice reorganization.

Introduction

The spin crossover phenomenon, first reported by Cambi *et al.* with tris(*N*,*N*-dialkyl-dithio-carbamato)iron(III) compounds,[1] has been later characterized for numerous $3d^4$–$3d^7$ transition metal complexes. This field of molecular magnetism[2] has been investigated extensively and provided spectacular examples of molecular bistability. Cooperative spin transitions and occurrence of hysteresis effects, described mainly for ferrous compounds,[3] are of interest for material science, both from a fundamental and an applied standpoint. For a majority of ferric systems, thermally activated spin-equilibria have been also reported,[4] and their roles in biological systems are of prime importance.[5]

We recently reported a cooperative $S = 1/2 \leftrightarrow S = 5/2$ spin-conversion process with hysteretic behavior in a ferric thiosemicarbazone complex, $Li[Fe(5BrThsa)_2]\cdot H_2O$ (H_2-5BrThsa being the 5-bromosalicylaldehyde thiosemicarbazone, see Chart 1).[6]

This compound belongs to a family of ferric complexes that provides interesting examples of cooperative processes.[7–14] When isolated as a water solvate, the title complex, $Li[Fe(5BrThsa)_2]\cdot H_2O$, undergoes a discontinuous spin transition with a rather broad hysteresis ($\Delta T = 39$ K) centred near room temperature (see Fig. 1). In contrast, the anhydrous material displays only a continuous transition.[8] The high-spin (HS) ↔ low-spin (LS) conversion of $Li[Fe(5BrThsa)_2]\cdot H_2O$ is associated with lattice reorganization: powder X-ray diffraction investigations have shown the occurrence of a crystallographic first-order phase transition coupled to the electronic spin state transition.[6,14] On the basis of temperature dependent IR measurements, it has been proposed that the phase transformation is associated with the modification of a hydrogen-bond network (see Fig. S1 in the ESI†). In the absence of a quality crystal for single crystal X-ray diffraction, we considered analysing the structural properties by powder X-ray diffraction techniques. As shown for a number of materials over the past ten years, this technique is a powerful tool that provides very valuable structural characterisations.[15]

We present here the powder structural resolution of the high- and low-temperature phases of $Li[Fe(5BrThsa)_2]\cdot H_2O$ in order to (i) determine the molecular structure of the anionic ferric complex (ii) analyze packing parameters associated with the discontinuous spin transition and the concomitant phase transition and (iii) identify the intermolecular contacts

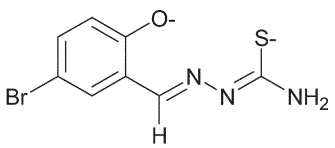

Chart 1 $5BrThsa^{2-}$ ligand.

[a] *ICMMO, Equipe de Chimie Inorganique, UMR 8182, Université Paris-Sud, 91400 Orsay, France. E-mail: mboillot@icmo.u-psud.fr*
[b] *Institut Lavoisier de Versailles, UMR 8180, Université de Versailles, 45 avenue des Etats-Unis, 78035 Versailles, France. E-mail: sebastien.floquet@uvsq.fr*
[c] *Centre de Physique Moléculaire Optique et Hertzienne, UMR 5798, Université Bordeaux I, Talence, France*

† Electronic supplementary information (ESI) available: Variable temperature IR spectra of compound $Li[Fe(5BrThsa)_2]\cdot H_2O$ (Fig. S1); distortions of the $[FeN_2O_2S_2]$ core in HS and LS phases and the structureless whole pattern profile refinements undertaken at 150 K and 373 K (Fig. S2 and S3); sphere angles and cell parameters of some HS or LS thiosemicarbazone ferric complexes (Tables S1 and S2). See DOI: 10.1039/b605326b.

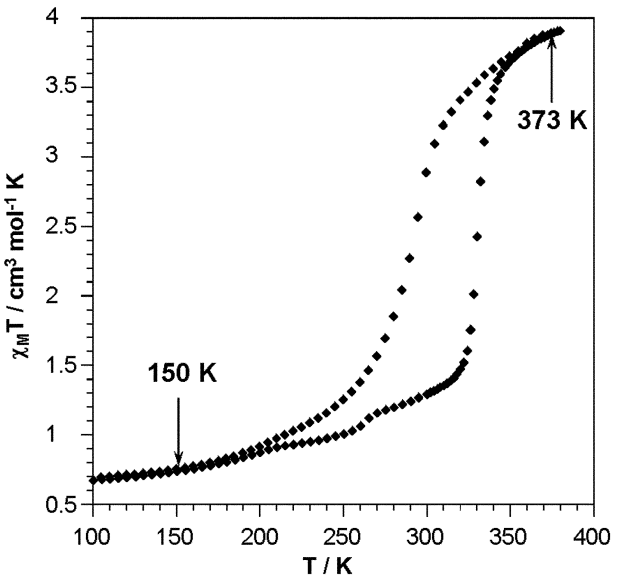

Fig. 1 Temperature dependence of the $\chi_M T$ product for Li[Fe(5BrThsa)$_2$]·H$_2$O.

between complexes which are the origin of the large asymmetric hysteretic loop of this compound.

Results and discussion

Magnetic measurements

In Fig. 1 is shown the temperature dependence of the $\chi_M T$ product (χ_M being the molar magnetic susceptibility) of Li[Fe(5BrThsa)$_2$]·H$_2$O. The discontinuous $S = 1/2 \leftrightarrow S = 5/2$ transition is associated with a broad asymmetric hysteresis loop ($T_C\downarrow$ = 292 K and $T_C\uparrow$ = 329 K). The $\chi_M T$ values of 0.63 cm^3 mol^{-1} K at 50 K and 3.91 cm^3 mol^{-1} K at 383 K correspond to 3% and 88% fractions of HS species, respectively, which indicates that the transition is near complete.

The hysteretic behaviour stems from a first-order crystallographic phase transition occurring upon spin crossover, as evidenced by DSC and routine XDP measurements.[6] Moreover, the very small step detected near 260 K in the heating curve (see Fig. 1) was previously assigned to an amorphous phase of Li[Fe(5BrThsa)$_2$]·H$_2$O, which was not evidenced by X-ray powder diffraction.

To conclude, the magnetic behaviour of Li[Fe(5BrThsa)$_2$]·H$_2$O clearly shows the dramatic influence of a solvent molecule as the solvent-free compound exhibits a continuous spin-crossover process.[8]

For instance, while a number of ferrous complexes exhibit a LIESST effect, very few ferric complexes are known to possess light induced properties.[16] Investigation of the LIESST effect has been carried out on Li[Fe(5BrThsa)$_2$]·H$_2$O at low temperature (10 K) and various excitation wavelengths. Unfortunately, no significant light-induced conversion of LS complexes to the metastable HS state was evidenced. It's well known that ferric complexes exhibit fast relaxation processes of the metastable HS state. It's thus difficult to observe the LIESST effect for these complexes. Moreover, the colour of our compound (dark brown to black) is probably not favourable to obtain a satisfactory excitation of the sample.

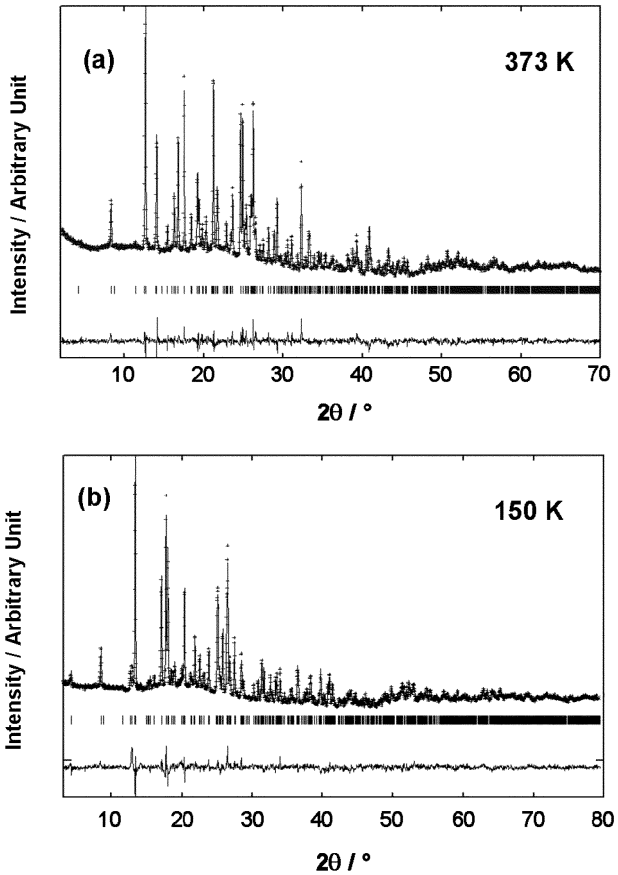

Fig. 2 Final Rietveld plots of the HS phase (a) and LS phase (b). The experimental data are shown by dots and the calculated pattern by a solid line. Difference curves are represented below; vertical bars mark the Bragg reflection positions.

HS structure at 373 K

Fig. 2a shows the final Rietveld refinement of the 373 K XDP of Li[Fe(5BrThsa)$_2$]·H$_2$O. This compound crystallises in the monoclinic system $P2_1/c$, with cell parameters given in Table 1 and selected angles and distances in Tables 2 and 3, respectively. The molecular structure refinement was carried out by letting bond angles free and allowing bond distances to vary slightly around mean values reported in the literature for similar HS ferric complexes. Analysis of the results is then based on the bond angles, whose values strongly depend on the metal ion spin states.[14,17]

The molecular structure of [Fe(5BrThsa)$_2$]$^-$ at 373 K is given in Fig. 3. The two tridentate ligands are placed around the metal ion in a meridional fashion. The coordination [FeO$_2$N$_2$S$_2$] core consists of two oxygen atoms (phenolate), two nitrogen atoms (imine) in *trans* disposition, and two sulfur atoms. The distortion of the coordination polyhedron is evidenced by bond angles deviating significantly from 90° (see Table 2 and Fig. S2a in the ESI†). It results from the constraints imposed by the interconnected five- and six-membered chelate cycles and the non-equivalent metal–ligand

Table 1 Crystallographic data for $Li[Fe(5BrThsa)_2]\cdot H_2O$ at 373 and 150 K

Formula	$LiFe(BrC_8H_6N_3OS)_2\cdot H_2O$	
Chemical formula weight/g mol^{-1}	625.05	
T/K	373	150
Calculated density/g cm^{-3}	1.849	1.981
Crystal system	Monoclinic	Monoclinic
Space group	$P2_1/c$	$P2_1/c$
a/Å	21.554(1)	20.715(2)
b/Å	11.479(1)	11.397(1)
c/Å	8.943(1)	8.880(1)
β/°	101.235(2)	90.258(2)
V/Å^3	2170.2(2)	2096.5(3)
M_{20}	16	19
F_{20}	37(0.0092; 59)	42(0.0066; 73)
Z	4	4
Radiation	Cu Kα_1	Cu Kα_1
2 θ range/°	2.17–70	3.18–79.5
No. reflections	946	1253
No. atoms	30	30
No. structural parameters	91	91
R_P, R_{WP}	0.019, 0.025	0.022, 0.031
R_I, R_F	0.082, 0.069	0.094, 0.063
R_{exp}	0.009	0.010

bonds (see selected data in Table 3). The twelve polyhedron angles of $[Fe(5BrThsa)_2]^-$ at 373 K are close to those reported for the HS ferric complex $Cs[Fe(Thsa)_2]$[9] (see Table S1 in the ESI†).

The molecular characteristics of the HS species being determined, packing and intermolecular interactions can be analysed in order to identify structural parameters favouring the cooperative interactions, hydrogen bonding or π-stacking interactions.[16,18] Fig. 4a displays the molecular packing along the b axis. The complexes are organised in layers that are parallel to the bc plane and separated by the hydrophobic component of the ligand (bromo substituted aromatic rings). Within the bc planes, a frame of metal ions separated by 7.22, 7.34 and 8.94 Å is observed. The inter-plane distances are alternatively equal to 10.55 and 11.07 Å. No π-stacking interaction can be identified in the HS lattice. In Table 4 are reported the interatomic distances that are smaller than the sum of the van der Waals radii. The O(w1) oxygen atom of H_2O is involved in moderate intermolecular contacts with the

Table 2 Selected angles (°) for $Li[Fe(5BrThsa)_2]\cdot H_2O$ at 373 and 150 K

T/K	373	150
O(1)FeO(2)	76(2)	81(2)
O(1)FeS(2)	101(2)	92(2)
O(1)FeN(11)	83(2)	88(2)
O(1)FeN(21)	110(2)	96(2)
O(2)FeS(1)	94(1)	99(2)
O(2)FeN(11)	107(2)	97(2)
O(2)FeN(21)	81(2)	84(2)
S(1)FeS(2)	97(1)	90(1)
S(1)FeN(11)	80(2)	83(2)
S(1)FeN(21)	89(1)	94(2)
S(2)FeN(11)	94(1)	93(2)
S(2)FeN(21)	80(1)	86(2)
O(1)FeS(1)	156(2)	171(2)
O(2)FeS(2)	158(2)	167(2)
N(11)FeN(21)	166(2)	178(2)

Table 3 Selected bond lengths (Å) for $Li[Fe(5BrThsa)_2]\cdot H_2O$ at 373 and 150 K

T/K	373	150
Fe–S(1)	2.35(2)	2.24(2)
Fe–S(2)	2.35(2)	2.26(2)
Fe–O(1)	1.93(3)	1.94(3)
Fe–O(2)	1.97(3)	1.93(3)
Fe–N(11)	2.18(2)	1.98(2)
Fe–N(21)	2.16(2)	1.99(2)

N(12) nitrogen atom of the N–N group (2.91(5) Å) and the O(2) and O(1) phenolate oxygen atoms (2.99(5) and 3.07(5) Å, respectively). Other intermolecular contacts are also observed: N(13)···Br(2) = 3.25(5) Å, N(23)···O(1) = 3.09(5) Å, and N(23)···Br(1) = 3.61(5) Å. Although the nature of these interactions (van der Waals contacts, hydrogen bonds) cannot be identified confidently, the distance between O_w and N_{amine} atoms strongly suggests the existence of hydrogen bonds, a feature already pointed out by IR measurements[6,14] (see Fig. S1 in the ESI†). Note that the strongest intermolecular contacts are localised in the molecular planes that are parallel to bc planes (see Fig. 5), whereas the weakest interactions are observed between consecutive planes.

LS structure at 150 K

Fig. 2b shows the final refinement of the XDP at 150 K. This crystal structure (pseudo-orthorhombic system) is similar to that of $NH_4[Fe(5BrThsa)_2]$[10] and $NH_4[Fe(5ClThsa)_2]$[11] (orthorhombic systems, see Table S2 in the ESI†). The space group remains $P2_1/c$ (Table 1), despite the occurrence of a crystallographic phase transition, as characterized by DSC and powder XDP studies.[6] Both the cell parameters and molecular packing show dramatic changes upon temperature decrease (Fig. 4b). The decrease of β from 101.2° at 373 K to 90.2° at 150 K is associated with changes of the complex

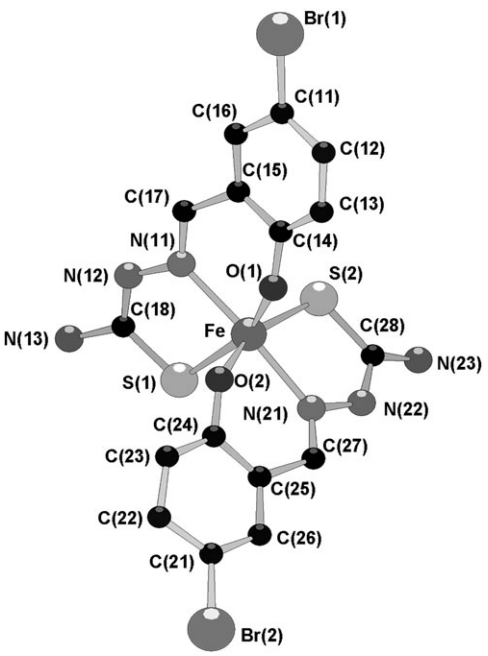

Fig. 3 Structure of the $[Fe(5BrThsa)_2]^-$ anion at 373 K.

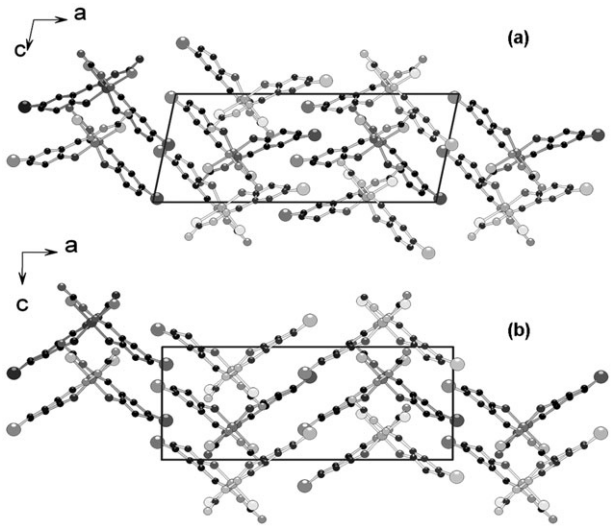

Fig. 4 Comparison of unit cells of HS (a) and LS (b) phases along the *b* axis. Water molecules have been omitted for clarity.

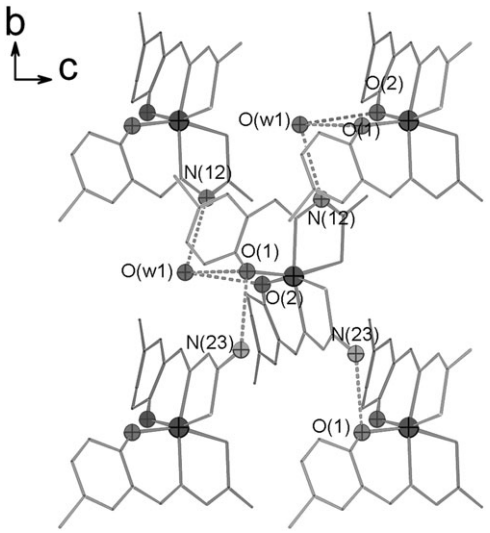

Fig. 5 Strongest intermolecular contacts between complexes at 373 K.

coordinates in the unit cell and with different positions of the heavy atoms in both phases. These observations account for the differences shown in Fig. 2a and b between the high- and low-temperature XDP.

The decrease in the unit cell volume from 2170.2(2) $Å^3$ at 373 K to 2096.5(3) $Å^3$ at 150 K corresponds to a *ca.* 18.5 $Å^3$ volume variation per formula unit ($Z = 4$). This rather small value corresponds to both lattice thermal contraction and spin crossover. We note that the *ca.* 3.5% relative variation of the unit cell volume upon spin change is of same magnitude to values reported for iron(II) and iron(III) spin-crossover complexes.[17]

The HS to LS change of the metal ion is associated with a net reorganization of the molecular structure. Consistent with literature reports,[17,19] the coordination angles become closer to 90° and the distortion of the pseudo-octahedral $[FeN_2O_2S_2]$ core is reduced at lower temperature (see Fig. S2b and Tables 2 and 3). In addition, we note a reasonable agreement between the polyhedron angles of $Li[Fe(5BrThsa)_2]\cdot H_2O$ and the values reported by Ryabova *et al.* for similar LS species[10–12] (see Table S1 in the ESI†).

In contrast to the moderate variation of the unit cell volume, drastic changes of the packing and intermolecular interactions occur over the phase transition (see Table 4 and Fig. 4–6). As described above, the molecular packing consists of layers of ferric complexes (in *bc* plane). Within each layer, the ferric complexes are closely packed with alignments of metal ions alternately separated by 7.13 and 7.31 Å. The different planes containing the ferric complexes are spaced along *a* axis by *ca.* 11.33 and 10.74 Å. The intermolecular contacts, mainly observed in the *bc* planes, differ from those characterised in the high temperature phase. Strong interactions are observed between oxygen and nitrogen atoms: for example between the phenolate O(1) and amine N(23) atoms, O(1)···N(23) = 2.65(5) Å, and between the water O(w1) and imine N(22) atoms, O(w1)···N(22) = 2.71(5) Å (Fig. 6). In parallel, the intermolecular contacts between some N and Br atoms decrease: N(13)···Br(2) = 3.25(5) Å (373 K), 3.53(5) Å (150 K) and N(23)···Br(1) = 3.61(5) Å (373 K), 3.83(5) Å (150 K).

Different features can be inferred from this set of observations. A modulation of the electronic density on the phenolate

Table 4 Selected distances (Å) corresponding to intermolecular contacts in $Li[Fe(5BrThsa)_2]\cdot H_2O$ at 373 and 150 K. Values in brackets are given for comparison

T/K	373	150
O(w1)–N(12)	2.91(5)	(3.53(5))
O(w1)–N(22)	(3.33(5))	2.71 (5)
O(w1)–O(1)	3.07(5)	3.01(5)
O(w1)–O(2)	2.99(5)	3.00(5)
N(13)–O(2)	(3.41(5))	3.23(5)
N(13)–Br(2)	3.25(5)	3.53(5)
N(23)–O(1)	3.09(5)	2.65(5)
N(23)–Br(1)	3.61(5)	(3.83(5))

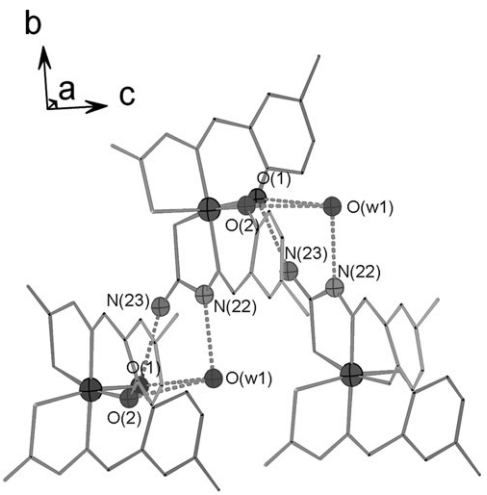

Fig. 6 Strongest intermolecular contacts between complexes at 150 K.

oxygen atom can be expected from the O(1)···N(23) contact. Accordingly, variable temperature FT-IR measurements[6] strongly suggest the presence of hydrogen bonding interactions (see Fig. S1 in the ESI†) and that the nature and strength of these interactions are modified during the crystallographic phase transition. We note that the most cooperative process is observed from the conversion of the low-temperature lattice, *i.e.* the phase with the strongest intermolecular contacts. Consequently, the cooperative character of the transition is related to strong elastic interactions[20] exerted on the LS species, these being partly mediated by the water molecules.

Conclusion

The crystal structure of $Li[Fe(5BrThsa)_2]\cdot H_2O$ was determined from powder X-ray diffraction data at temperatures corresponding to the LS and HS phases. The spin crossover of $Li[Fe(5BrThsa)_2]\cdot H_2O$ is concomitant to a first-order crystallographic phase transition. This process takes place without any space group modification. The anionic complexes are implicated in several intermolecular interactions involving N, O, Br atoms and the water molecules. The water molecule likely interacts through hydrogen bonds, as evidenced previously by IR. A significant variation of the water-mediated interactions is detected between the low- and the high-temperature phases. Thus, the occurrence of a cooperative process and of a crystallographic phase transition can be related to the existence of a supramolecular network involving water molecules whose interactions with the ferric units are switched upon the thermal spin-crossover process.

Finally, this work confirms that the thiosemicarbazone ferric complexes are good candidates for studying the cooperative spin-crossover processes of Fe(III) and form very attractive building blocks for the elaboration of novel multifunctional molecular materials.

Experimental

Syntheses and characterization

The ferric complex $Li[Fe(5BrThsa)_2]\cdot H_2O$, prepared as previously described,[6] was characterized by FT-IR, ES-MS and elemental analysis. ES-MS (MeOH): m/z = 599.9 (calcd for $[Fe(5BrThsa)_2]^-$: 600.1). Anal. Calcd (Found) for $Li[Fe(5BrThsa)_2]\cdot H_2O$: C 30.75 (30.73); H 2.26 (2.27); N 13.45 (13.27); S 10.26 (10.54); Fe 8.93 (8.32); Li 1.11 (0.93). The magnetic behaviour of $Li[Fe(5BrThsa)_2]\cdot H_2O$ was determined by a Quantum Design SQUID magnetometer (MPMS5S).

High resolution X-ray diffraction patterns (XDP)

X-Ray high-resolution diffraction patterns were recorded by means of a horizontally mounted INEL cylindrical position sensitive detector (CPS 120) using Debye–Scherrer geometry (angular step *ca.* 0.029°–2θ).[21] Monochromatic Cu Kα_1 radiation was selected as incident beam. Low temperature measurements were achieved with an Oxford Cryosystems N_2 cryostream which provides isothermal experiments at different temperatures. The generator power was set to 40 kV and 25 mA. Samples were introduced in 0.5 mm diameter Lindemann rotating glass capillaries in order to minimize preferential orientations of the crystallites. The time of acquisition was set to seven hours in order to obtain reflections with exploitable intensities. External calibration using $Na_2Ca_3Al_2F_{14}$[22] cubic phase combined with a low-angle calibration using silver behenate[23] was performed by means of cubic spline fittings.

Structure determination from X-ray powder diffraction

X-Ray data analyses and indexing. The same strategy was used for both phases. Extraction of the peak positions was performed by means of the WinPLOTR program.[24] Patterns indexing was carried out with the computer program DICVOL04[25] from the twenty unambiguous first lines, with an absolute error on peak positions of 0.03° (2θ). Monoclinic solutions were found with satisfactory figures of merit (see Table 1) and confirmed by successful indexing of all input lines. Systematic absences ($0k0$, $k = 2n + 1$ and $h0l$, $l = 2n + 1$) were consistent with the $P2_1/c$ space group. Adequacy of unit cells and space group was confirmed by structureless whole pattern profile refinements by the Le Bail method[26] integrated in the FullProf program.[27]

High-spin phase. First calculations were performed with the EXPO[28] package, integrating EXTRA[29] for extracting integrated intensities and SIR97[30] for direct methods structure solution. A list of 1327 reflections was extracted in the angular range 2.17–80° (2θ). According to the degree of diffraction overlap, 16.60% of these reflections were statistically considered as independent. No preferred orientation effects have been found. The two Br and Fe atoms were found unambiguously from the E-map with the highest figure of merit. Orientations of the two independent organic moieties were then determined by using the direct space strategy program FOX,[31] choosing the parallel tempering algorithm. The use of 3 objects (two organic molecules and one Fe atom), using starting positions found by SIR97, restricts the number of parameters to 6 (3 for the orientation of each organic) in comparison with 78 atomic coordinates corresponding to the 26 remaining atoms of the complex. To avoid objects overlapping, anti-bumping restraints (Fe–O and Fe–N: 1.7 Å; Fe–S: 1.9 Å) were applied. Calculations converged in almost 2 h to the expected solution. The corresponding atomic coordinates were used as the starting model for Rietveld refinement, using the FullProf[27] program integrated in WinPLOTR[24] software. A pseudo-Voigt function was selected to describe individual line profiles. In order to describe the angular dependence of the peak full-width at half maximum, the usual quadratic function in tan θ was used. Unit cell and instrumental parameters were allowed to vary from time to time during the refinement process, as well as atomic coordinates with soft distance and angular restraints. At this stage of the refinement, the structural model indicators converged to R_I = 0.174 and R_F = 0.084, which confirmed the validity of the starting structural hypothesis. Difference Fourier calculations were then undertaken by using SHELXL[32] and revealed unambiguously the water molecule.

Low-spin phase. The same softwares were used to solve the structure of the LS phase. According to the degree of

diffraction overlap, 20.24% of the 1283 reflections extracted in the angular range 2.17–80° (2θ) were statistically considered as independent and used for direct-methods calculations. The Br and Fe atoms with four donor atoms (S and O atoms) were found from the E-map with the highest figure of merit. The same three objects were considered in the Fox program. As for the HS phase, bromide atoms were first used as pivot atoms for organic moieties, but calculations never converged, due to some inaccuracy on their positions. Organic molecules were then allowed to rotate around sulfur atoms instead of the bromide atom and calculations converged rapidly to the correct structural model. The water molecule was also localized by difference Fourier calculations alternating with Rietveld refinement cycles.

Final Rietveld refinements. Final Rietveld refinements (see Table 1) carried out in angular ranges 2.17–70°(2θ) and 3.18–79.5° (2θ) used 946 and 1253 reflections for the HS and LS phase, respectively. They involved the following parameters: 90 atomic coordinates, 1 scale factor, 1 zero-point, 4 cell parameters and 2 half-width parameters for both phases. One variable for η was refined for the HS phase and 2 asymmetry factors were also considered for the BS phase. Soft distances and angular restraints were maintained for ligands in both phases. Background has been treated as linear interpolation between 39 and 34 given points for high- and low-temperature phases, respectively. As a first convergence criterion, the metal–ligand bond lengths were allowed to slightly vary around the average values reported in literature for HS and LS species.[9–13] Attempts to localize the Li^+ cations were not undertaken. Indeed, lithium scattering strength is insignificant compared to the ferric complex. Moreover, last difference Fourier calculations undertaken for the both phases confirms that no additional atom can be localized. Fig. 2 shows the final fits obtained between calculated and observed patterns. They correspond to satisfactory crystal structure model indicators and profile factors (R_I and R_F, see Table 1). In powder diffraction, the R_p and R_{wp} factors are not the most relevant factors to confirm the validity of the fits. Indeed, in our study for example, it is clear that R_p and R_{wp} are "artificially" lowered by high background levels. Nevertheless, R_I and R_F values are satisfactory (less than 10%) and the R_I/R_F ratios are lower than 1.5, indicating that structural models are complete. These values demonstrate the accuracy of the two structural models. Finally, structureless whole pattern profile refinements have been undertaken at 150 and 373 K (see Fig. S3 in the ESI†). The difference curves are not significantly improved compared to the Rietveld refinement, which confirms the accuracy of the present structural models. CCDC reference numbers 617382 and 617383. For crystallographic data in CIF or other electronic format see DOI: 10.1039/b605326b

Acknowledgements

We thank Dr Michel Gasgnier for preliminary investigations and Dr Xavier Ottenwaelder for help in the preparation of the revised version of this manuscript. Financial support from the European Union (TOSS TMR, Contract ERB-FMRX-CT98-0199) and (MAGMANet NoE, Contract NMP3-CT-2005-515767-2) are gratefully acknowledged.

References

1 (*a*) L. Cambi and A. Cagnasso, *Atti. Accad. Naz. Lincei, Cl. Sci. Fis. Mat. Nat. Rend.*, 1931, **13**, 809; (*b*) L. Cambi and L. Szegö, *Ber. Dtsch. Chem. Ges.*, 1931, **64**, 167.
2 (*a*) *Topics in Current Chemistry, Spin Crossover in transition metal compounds*, ed. P. Gütlich and H. A. Goodwin, Springer, Berlin, 2004, vol. 233–235; (*b*) O. Kahn, *Molecular Magnetism*, VCH, New York, 1993.
3 P. Gütlich, A. Hauser and H. Spiering, *Angew. Chem., Int. Ed. Engl.*, 1994, **33**, 2024.
4 P. J. van Koningsbruggen, Y. Maeda and H. Oshio, in *Spin Crossover in Transition Metal Compounds I, Topics in Current Chemistry*, ed. P. Gütlich and H. A. Goodwin, Springer, Berlin, 2004, vol. 233, pp. 259–324.
5 W. R. Sheidt and C. A. Reed, *Chem. Rev.*, 1981, **81**, 543.
6 S. Floquet, M.-L. Boillot, E. Rivière, F. Varret, K. Boukheddaden, D. Morineau and P. Négrier, *New J. Chem.*, 2003, **27**, 341–348.
7 (*a*) V. V. Zelentsov, *Sov. Sci. Rev. Sect. B, Chem.*, 1987, **10**, 485; (*b*) V. V. Zelentsov, *Sov. J. Coord Chem.*, 1992, **18**, 787; (*c*) M. D. Timken, S. R. Wilson and D. N. Hendrickson, *Inorg. Chem.*, 1985, **24**, 3450; (*d*) M. Mohan, P. H. Madhuranath, A. Kumar and N. K. Jha, *Inorg. Chem.*, 1989, **28**, 96; (*e*) N. S. Gupta, M. Mohan, N. K. Jha and W. E. Antholine, *Inorg. Chim. Acta*, 1991, **184**, 13.
8 V. V. Zelentsov, L. G. Bogdanova, A. V. Ablov, N. V. Gerbeleu and C. V. Dyatlova, *Russ. J. Inorg. Chem. (Engl. Trans.)*, 1973, **18**, 1410.
9 N. A. Ryabova, V. I. Ponomarev, V. V. Zelentsov and L. O. Atovmyan, *Sov. Phys. Crystallogr. (Engl. Transl.)*, 1981, **26**, 53–57.
10 N. A. Ryabova, V. I. Ponomarev, V. V. Zelentsov, V. I. Shipilov and L. O. Atovmyan, *J. Struct. Chem. (Engl. Transl.)*, 1981, **22**, 234.
11 N. A. Ryabova, V. I. Ponomarev, L. O. Atovmyan, V. V. Zelentsov and V. I. Shipilov, *Sov. J. Coord. Chem. (Engl. Transl.)*, 1978, **4**, 95.
12 N. A. Ryabova, V. I. Ponomarev, V. V. Zelentsov and L. O. Atovmyan, *Sov. Phys. Crystallogr. (Engl. Transl.)*, 1982, **27**, 171–175.
13 (*a*) N. A. Ryabova, V. I. Ponomarev, V. V. Zelentsov and L. O. Atovmyan, *Sov. Phys. Crystallogr. (Engl. Transl.)*, 1982, **27**, 46–52; (*b*) N. A. Ryabova, V. I. Ponomarev, V. V. Zelentsov and L. O. Atovmyan, *Dokl. Chem. (Engl. Transl.)*, 1981, **259**, 715–719.
14 S. Floquet, PhD Thesis, University of Paris XI, 2001.
15 K. D. M. Harris, M. Tremayne and B. M. Kariuki, *Angew. Chem., Int. Ed.*, 2001, **40**, 1626.
16 S. Hayami, Z.-Z. Gu, M. Shiro, Y. Einaga, A. Fujishima and O. Sato, *J. Am. Chem. Soc.*, 2000, **122**, 7126–7127.
17 (*a*) E. König, *Prog. Inorg. Chem.*, 1987, **35**, 527; (*b*) P. Guionneau, C. Brigouleix, Y. Barrans, A. E. Goeta, J.-F. Létard, J. A. K. Howard, J. Gaultier and D. Chasseau, *C. R. Acad. Sci., Ser. IIc: Chim.*, 2001, **4**, 161–171; (*c*) P. Guionneau, J.-F. Létard, D. S. Yufit, D. Chasseau, G. Bravic, A. E. Goeta, J. A. K. Howard and O. Kahn, *J. Mater. Chem.*, 1999, **9**, 985–994.
18 (*a*) J.-F. Létard, P. Guionneau, L. Rabardel, J. A. K. Howard, A. E. Goeta, D. Chasseau and O. Kahn, *Inorg. Chem.*, 1998, **37**, 4432–4441; (*b*) A. M. Greenaway and E. Sinn, *Inorg. Chem.*, 1978, **100**, 8080–8084; (*c*) P. Gütlich, H. Köppen and H. G. Steinhäuser, *Chem. Phys. Lett.*, 1980, **74**, 475.
19 (*a*) H. Oshio, K. Toriumi, Y. Maeda and Y. Takashima, *Inorg. Chem.*, 1991, **30**, 4252–4260; (*b*) A. J. Conti, R. K. Chadha, K. M. Sena, A. L. Rheingold and D. N. Hendrickson, *Inorg. Chem.*, 1993, **32**, 2670–2680; (*c*) A. J. Conti, K. Kaji, Y. Nagano, K. M. Sena, Y. Yumoto, R. K. Chadha, A. L. Rheingold, M. Sorai and D. N. Hendrickson, *Inorg. Chem.*, 1993, **32**, 2681–2693.
20 H. Spiering, in *Spin Crossover in Transition Metal Compounds I Topics in Current Chemistry*, ed. P. Gütlich and H. A. Goodwin, Springer, Berlin, 2004, vol. 235, pp. 171–195.
21 J. Ballon, V. Comparat and J. Pouxe, *Nucl. Instrum. Methods*, 1983, **217**, 213.

22 M. Evain, P. Deniard, A. Jouanneaux and R. Brec, *J. Appl. Crystallogr.*, 1993, **26**, 563.
23 T. C. Huang, H. Toraya, T. N. Blanton and Y. Wu, *J. Appl. Crystallogr.*, 1993, **26**, 180.
24 T. Roisnel and J. Rodriguez-Carvajal, *Mater. Sci. Forum*, 2001, **378–381**, 118.
25 A. Boultif and D. Louër, *J. Appl. Crystallogr.*, 2004, **37**, 724.
26 A. Le Bail, H. Duroy and J. F. Fourquet, *Mater. Res. Bull.*, 1988, **23**, 447.
27 J. Rodriguez-Carvajal, *Collected Abstracts of Powder Diffraction Meeting*, Toulouse, France, 1990.
28 A. Altomare, M. C. Burla, M. Camalli, B. Carrozzini, G. L. Cascarano, C. Giacovazzo, A. Guagliardi, A. G. G. Moliterni, G. Polidori and R. Rizzi, *J. Appl. Crystallogr.*, 1999, **32**, 339.
29 A. Altomare, M. C. Burla, G. Cascarano, C. Giacovazzo, A. Guagliardi, A. G. G. Moliterni and G. Polidori, *J. Appl. Crystallogr.*, 1995, **28**, 842.
30 A. Altomare, M. C. Burla, M. Camalli, G. L. Cascarano, C. Giacovazzo, A. Guagliardi, A. G. G. Moliterni, G. Polidori and R. Spagna, *J. Appl. Crystallogr.*, 1999, **32**, 115.
31 V. Favre-Nicollin and R. Cerny, *J. Appl. Crystallogr.*, 2002, **35**, 734.
32 G. M. Sheldrick, *SHELXL97*, University of Göttigen, Germany, 1997.